ACS OMEGA

http://pubs.acs.org/journal/acsodf

Article

Effect of Silane Monolayers and Nanoporous Silicon Surfaces on the Matrix-Assisted Laser Desorption Ionization Mass Spectrometry Detection of Sepsis Metabolites Biomarkers Mixed in Solution

Antonin Lavigne, Thomas Géhin, Benoît Gilquin, Vincent Jousseaume, Marc Veillerot, Claude Botella, Céline Chevalier, Cécile Jamois, Yann Chevolot, Magali Phaner-Goutorbe, and Christelle Yeromonahos*

Cite This: *ACS Omega* 2023, 8, 28898−28909

Read Online

ABSTRACT: Matrix-assisted laser desorption ionization time-of-flight mass spectrometry (MALDI-ToF MS) is a promising strategy for clinical diagnosis based on metabolite detection. However, several bottlenecks (such as the lack of reproducibility in analysis, the presence of an important background in low-mass range, and the lack of organic matrix for some molecules) prevent its transfer to clinical cases. These limitations can be addressed by using nanoporous silicon surfaces chemically functionalized with silane monolayers. In the present study, sepsis metabolite biomarkers were used to investigate the effects of silane monolayers and porous silicon substrates on MALDI-ToF MS analysis (signal-to-noise value (S/N), relative standard deviation of the S/N of triplicate samples (STD_{mean}), and intra-substrates uniformity). Also, the impact of the physicochemical properties of metabolites, with different isoelectric points and hydrophobic−hydrophilic balances, was assessed. Four different silane molecules, with various alkyl chain lengths and head-group charges, were self-assembled in monolayers on plane and porous silicon surfaces. Their surface coverage and conformity were investigated by X-ray photoelectron spectroscopy (XPS) and time-of-flight secondary ion mass spectrometry (ToF-SIMS). The seven metabolites detected on the stainless-steel target plate (lysophosphatidylcholine, caffeine, phenylalanine, creatinine, valine, arginine, and glycerophosphocholine) are also detected on the silanized and bare, plane and porous silicon surfaces. Moreover, two metabolites, glycine and alanine, which are not detected on the stainless-steel target plate, are detected on all silanized surfaces, except glycine which is not detected on CH_3 short-modified porous silicon and on the bare plane silicon substrate. In addition, whatever the metabolites (except phenylalanine and valine), at least one of the silicon surfaces allows to increase the S/N value in comparison with the stainless-steel target plate. Also, the heterogeneity of matrix crystallization features is linked to the STD_{mean} which is poor on the NH_3^+ monolayer on plane substrate and better on the NH_3^+ monolayer on porous substrate, for most of the metabolites. Nevertheless, matrix crystallization features are not sufficient to systematically get high STD_{mean} and uniformity in MALDI-ToF MS analysis. Indeed, the physicochemical properties of metabolites and surfaces, limitations in metabolite extraction from the pores, and improvement in metabolite desorption due to the pores are shown to significantly impact MS analysis. In particular, in the case of the most hydrophobic metabolites studied, the highest S/N values and the best STD_{mean} and uniformity (the lowest values) are reached by using porous substrates, while in the case of the most hydrophilic metabolites studied, plane substrates demonstrated the highest S/N and the lowest STD_{mean}. No clear trend of surface chemistry was evidenced.

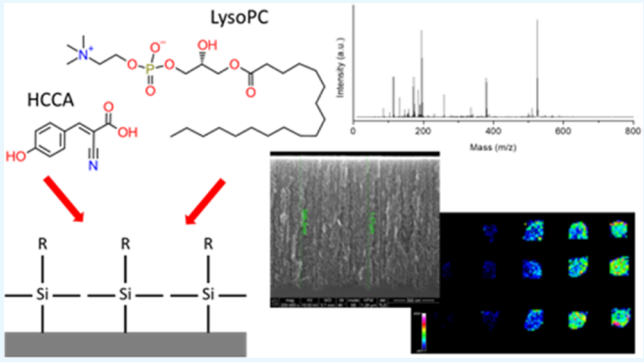

INTRODUCTION

Matrix-assisted laser desorption ionization time-of-flight mass spectrometry (MALDI-ToF MS) is a widely investigated strategy for the detection of low-molecular-weight metabolites (such as amino acids, lipids, sugars, organic acids, etc.), from fluids and biological tissues, with potential real-case clinical applications.[1−3] The matrix is central to the MALDI process, and the analyte incorporation, desorption, and ionization efficiencies can vary between given matrix/analyte pairs or from one shot to another due to the inhomogeneity of the spotted sample. Furthermore, the matrix generates an important background in the low-mass range of the mass spectra that limits the detection of low-molecular-weight ions.[4] The presence of "hot spots" where the analyte/matrix

Received: June 15, 2023
Accepted: July 7, 2023
Published: July 26, 2023

Table 1. Silane Molecules and Their Structural Formula

Silane denomination	Structural formula
CH_3 short	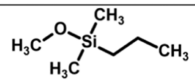
CH_3 long	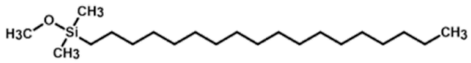
COO^-	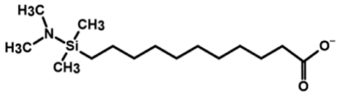
NH_3^+	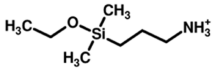

concentration is high can lead to repeatability issues which can be partially solved by developing matrix deposition methods that improve the uniformity of the matrix surface coverage.[5] Another concern of MALDI-ToF MS is the ion suppression caused, for example, by the presence of phospholipids that can impede the detection of some other metabolites such as neutral lipids.[5] Furthermore, for several metabolites, an efficient organic matrix is still lacking.[3] Therefore, the high throughput metabolite investigation of human fluids, for clinical diagnosis by MALDI, is still a challenge as it requires the simultaneous detection of a panel of species characterized by a large diversity of physicochemical properties, such as electrical charges and hydrophobic−hydrophilic balance.

To overcome these limitations, surface-assisted laser desorption/ionization (SALDI) techniques were developed. These matrix-free approaches are highly promising in clinical diagnosis based on metabolite profiling. Indeed, the high repeatability of analysis, low background in the low-mass range, and the simultaneous ionization of a large variety of analytes have been demonstrated.[6] Desorption/ionization on silicon (DIOS) is one of the most successful SALDI techniques to desorb and ionize metabolites. However, DIOS-MS signals are dramatically lower than MALDI-ToF MS signals. Based on the original DIOS method, Siuzdak et al. have developed nanostructured initiator mass spectrometry (NIMS).[7] NIMS differs from MALDI in that the analytes are not co-crystallized with the initiator and the UV energy is absorbed by the porous silicon leading to a rapid surface heating, vaporization of the trapped initiator, and desorption/ionization of the adsorbed analyte.[8] This strategy has demonstrated improved performance over DIOS-MS for metabolite detection.

Other authors have worked on hybrid techniques, combining MALDI and SALDI techniques. They have been proven highly efficient to maximize both ion intensity and the intra- and inter-substrate reproducibility in metabolite analysis while decreasing the background in the low-mass range.[9] In particular, matrix-enhanced NIMS (ME-NIMS), carried out by coating the porous silicon substrate with a layer of organic matrix, was shown to be a good alternative for the detection of phospholipids and small peptides.[10] Moreover, previous studies have shown that porous silicon substrates, with pore diameters in the range of 2−10 nm, enable the steric exclusion of large molecules from complex biological fluids, allowing direct MALDI-ToF MS analysis of plasma droplets, without any pretreatment steps. It allowed the discrimination of pathological samples (e.g., cardiovascular diseases) from nonpathological samples (through statistical analysis of the metabolite spectral pattern).[11−15] Furthermore, several studies have also shown that the MALDI-ToF signal is influenced by the surface chemistry of the substrate.[16−23] In particular, self-assembled monolayers of silane molecules on porous silicon surfaces seem to be well adapted to improve the MALDI-ToF MS detection of metabolites. For instance, Hsieh et al. have shown that 3-aminopropyltriethoxysilane functionalization increased the detection limit of bradykinin (904 g/mol) and gramicidin D (1882 g/mol), from 11 to 0.93 nM and from 110 to 0.33 μM, respectively, in the model solution.[24] A wide range of silane molecules are commercially available allowing to tune silicon surface physicochemical properties.[25−28] Furthermore, silanization processes can be industrialized at low cost and high throughput. Consequently, silanized porous silicon surfaces are highly promising for the development of clinical diagnosis tools based on metabolite trapping and MALDI-ToF MS detection, in a few minutes.

Nevertheless, to the best of our knowledge, the impact of porous silicon substrates versus plane silicon substrates and the impact of the alkyl chain length and head-group charges of silane molecules on MALDI-ToF MS detection of metabolites, characterized by various physicochemical properties, have never been investigated.

Herein, we aimed to address the impact of various silane monolayers on porous silicon on the signal-to-noise (S/N) ratio, on the relative standard deviation of the S/N of a triplicate sample (STD_{mean}), and on the intra-substrate uniformity of low-molecular-weight metabolites detected by MALDI-MS. To this aim, plane silicon substrates and porous silicon substrates were functionalized with four different silane molecules. Plane and porous silicon substrates are compared to decorrelate the effect of porosity from the effects of surface chemistry. The four silane molecules have long and short alkyl chains and the head groups were varied (Table 1). These molecules are 3-aminopropyldimethylethoxysilane (named NH_3^+ in this study), n-propyldimethylmethoxysilane (named CH_3 short), octadecyldimethylmetoxysilane (named CH_3 long), and *tert*-butyl-11-(dimethylamino(dimethyl)silyl)-undecanoate (leading to COO^- after deprotection). Twenty-five different metabolites (Table 2),[29−39] with different physicochemical properties (electrical charges and hydrophobic−hydrophilic balance), were analyzed by MALDI-ToF MS. Twenty-three of them are relevant sepsis biomarkers, and two of them are commonly found in the blood. The S/N ratio, STD_{mean}, and intra-substrates uniformity were evaluated as a

https://doi.org/10.1021/acsomega.3c04266
ACS Omega 2023, 8, 28898−28909

Table 2. 25 Metabolites Studied[a]

Lipids			
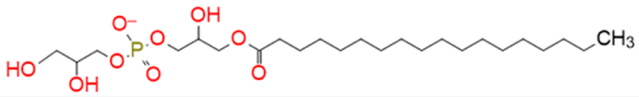	Lyso PG[29,30]	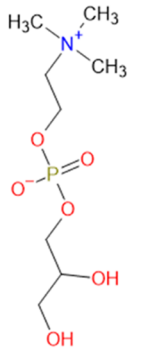	
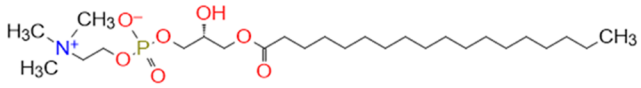	Lyso PC*[29-33]		
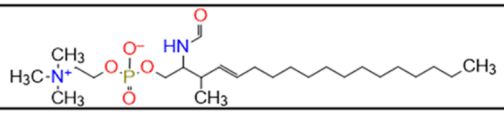	Sphingomyelin[29-30]		
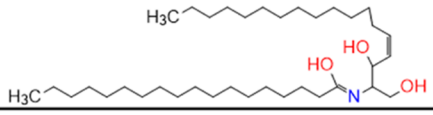	C18 Ceramide[29,33]		GPC*[29,30]
Acids			
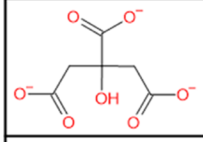	Citric Acid[29,34]	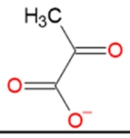	Pyruvic Acid[29,34]
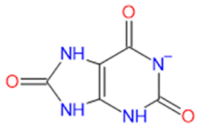	Uric acid[29]		
Amino acids and derivatives			
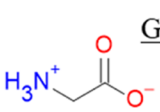	Glycine[29,35]	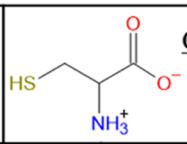	Cysteine[29,35]
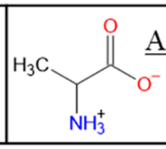	Alanine[29,35]	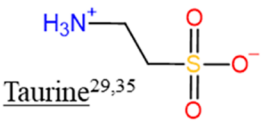	Taurine[29,35]
Methionine[29,35,36]	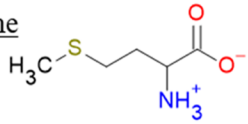	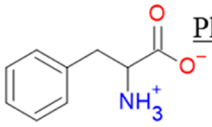	Phenylalanine*[29,35]
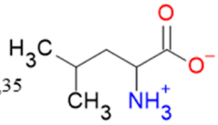	Leucine*[29,35]		
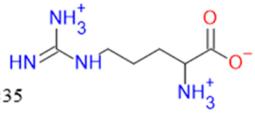	Arginine*[35]	Glutamine[29,35]	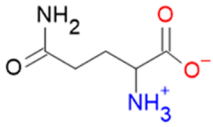
Citrulline[29,35]	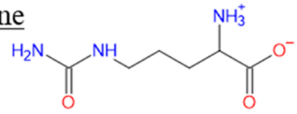		
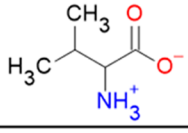	Valine*[29,35]	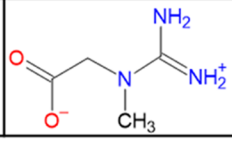	Creatine*
Tryptophan[29]	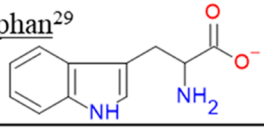		
Others			
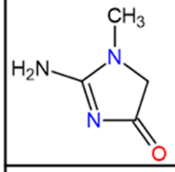	Creatinine*[29,37]	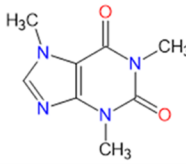	Caffeine*
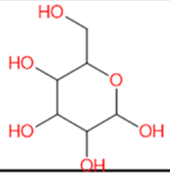	Glucose[38,39]		
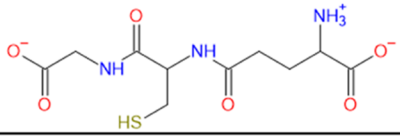	Glutathione[29]		

[a]23 metabolites specific to sepsis are underlined. The 9 metabolites detected simultaneously in this study using CHCA as a matrix are marked by a star (*). The reference numbers are indicated after the name of the metabolites. Lysophosphatidylcholine, lysophosphatidylglycerol, and glycerophosphocholine are respectively named LysoPC, LysoPG, and GPC in this study.

https://doi.org/10.1021/acsomega.3c04266
ACS Omega 2023, 8, 28898−28909

function of surface chemistry and porosity versus plane substrate.

First, the surface coverage of the different silane molecules, as well as the conformity of the different monolayers inside the pores, is characterized by X-ray photoelectron spectroscopy (XPS) and time-of-flight secondary ion mass spectrometry (ToF-SIMS). Then, six different organic matrices were compared. The preponderant discriminant criterion was the ability of the selected matrix to ionize the largest span of metabolites among the 25 metabolites studied. Indeed, profiling simultaneously metabolites can be regarded as a fingerprint of a specific illness.[29]

Among the six organic matrices, CHCA is shown to be the one that allows the simultaneous detection of the largest group of metabolites. Then, the S/N ratio, STD_{mean}, and intra-substrate uniformity for the different metabolites studied, on the different surfaces, were investigated and correlated to the heterogeneity of the CHCA matrix crystallization features. Finally, the impact of the physicochemical properties of metabolites (the octanol−water partition coefficient ($\log P$) and electrical charge) is evaluated by comparing the results obtained for the different metabolites detected simultaneously.

■ MATERIALS AND METHODS

Chemicals and Reagents. Porous silicon substrates were purchased from SiLiMiXT (Tours, France). Pores (10 nm in diameter and 1 μm in depth) were obtained through electrochemical etching of silicon substrates (150 mm in diameter, type P, 10−20 mΩ·cm, and 508 μm in thickness). The silane molecules studied were purchased from ABCR (Karlsruhe, Germany). *Tert*-butyl-11-(dimethylamino-(dimethyl)silyl)undecanoate was synthesized according to a protocol previously reported.[40] The 25 metabolites considered in this study were obtained from Sigma-Aldrich. The six organic matrices studied (α-cyano-4-hydroxycinnamic acid (CHCA), 2,5-dihydroxybenzoic acid (DHB), 9-aminoacridine (9AA), *N*-(1-naphthyl)ethylenediamine dihydrochloride (NEDC), 5-diaminonaphthalene (DAN), and 2,4,6-trihydroxyacetophenone monohydrate (THAP)) and the different solvents used (tetrahydrofuran 99% (THF), methanol, ethanol, chloroform, and trifluoroacetic acid (TFA)) were also obtained from Sigma-Aldrich. Acetonitrile (ACN) was purchased from Honeywell Riedel-de Haën.

Gas Phase Chemical Surface Functionalization. COO^- monolayers were prepared using the protocol previously reported by Phaner-Goutorbe et al.[41] For the three other silanes, the substrates were cleaned by ozone/ultraviolet treatment under an oxygen flow for 30 min at room temperature. Next, the substrates were placed under vacuum for 30 min at 150 °C and then cooled down at room temperature under a nitrogen atmosphere. 100 μL of silane was injected into the reaction chamber and the substrates were placed under vacuum while the temperature gradually increased to 150 °C (120 °C for NH_3^+). After 1 h of silanization, the chamber was cleaned thanks to a 15 min pumping, then the substrates were cooled down and put under nitrogen. Finally, the samples were washed for 10 min in THF and for 10 min in ultrapure water.

Matrix Preparation. The matrix solutions contain 10 mg/mL CHCA dissolved in a 0.1% solution of TFA in ACN/ultrapure water (60:40 v/v), 20 mg/mL DHB dissolved in 0.1% TFA in ACN/ultrapure water (30:70 v/v), 7 mg/mL NEDC in a solution of methanol/ultrapure water (50:50 v/v), 10 mg/mL THAP in a solution of ACN/ultrapure water (50:50 v/v) with diammonium hydrogen citrate 25 nM, and 10 mg/mL 9AA in an ethanol/ultrapure water solution (70:30 v/v). In the case of the 9AA matrix, the choice of solvent was based on the quality of crystals obtained, by Cerruti et al., for mass spectrometry imaging of metabolites.[42] For the test at different CHCA concentrations, 20 mg/mL CHCA was dissolved in a 0.1% solution of TFA in ACN/ultrapure water (60:40 v/v) before being diluted in the same solution to obtain the final concentrations (0, 1, 5, 10, and 20 mg/mL).

Preparation of Metabolites. LysoPC, LysoPG, sphingomyelin, and ceramide were dissolved in a chloroform/methanol solution (2:1 v/v) at 1 mg/mL. The 21 other metabolites were dissolved in ultrapure water at 1 mg/mL. The metabolites were mixed in equal volumes. The final concentration of each metabolite was 40 μg/mL.

MALDI-ToF MS Analysis. MALDI mass spectra were obtained using an UltrafleXtreme MALDI-TOF/TOF (Bruker Daltonics) equipped with a laser at 355 nm. Ions were detected in reflectron-positive (RP) or reflectron-negative (RN) ion mode at ±20 kV accelerating potential. The laser was set on medium size with a grid voltage of 80% in RP and 100% in RN ion mode. Samples were studied on an m/z range of 10−800. Analyses were done both on a classical stainless-steel MALDI target plate and silanized silicon substrates held on a modified target plate. 1 μL of the metabolite solution and 1 μL of the matrix solution were mixed, deposited on the MALDI plate or the silanized surfaces, and let crystallized in air before measurement. In the case of functionalized samples, an imagery of the evaporated droplet was performed using the FlexImaging 3.0 software (Bruker Daltonics) with a spatial resolution of 200 μm (40 spots per droplet). For each spot, 500 satisfactory laser shots were averaged to obtain a mass spectrum. The spectra were analyzed using the FlexAnalysis 3.4 software (Bruker Daltonics) for peak detection and for measuring the signal-to-noise ratios.

Statistical Analysis of MALDI-ToF MS Spectra. Each type of sample was done in triplicate. For each replicate of a given triplicate, the mean S/N ratio of each metabolite at $[M + H]^+$ was calculated from 40 different areas. Then, the mean of the three replicates was calculated as follows: S/N = [(mean of the 40 S/N values)$_{sample\text{-}1}$ + (mean of the 40 S/N values)$_{sample\text{-}2}$ + (mean of the 40 S/N values)$_{sample\text{-}3}$]/3. Moreover, the standard deviation of the means of the three replicates was calculated as follows: STD_{mean} = STD[(mean of the 40 S/N values)$_{sample\text{-}1}$; (mean of the 40 S/N values)$_{sample\text{-}2}$; (mean of the 40 S/N values)$_{sample\text{-}3}$]. Furthermore, for each replicate, the standard deviation of the 40 data points was calculated and averaged over the three replicates, which is in the following described as uniformity: uniformity = ($STD[S/N]_{40\_points\_sample\text{-}1}$ + $STD[S/N]_{40\_points\_sample\text{-}2}$ + $STD[S/N]_{40\_points\_sample\text{-}3}$)/3.

ToF-SIMS Profiling. High-resolution mass depth profiles were acquired by ToF-SIMS (ToF-SIMS V from ION-TOF). A bunched 15 keV Bi^{3+} ions was used as the primary probe for analysis (rastered area 80 × 80 μm^2) and sputtering was obtained using Cs^+ ions at low energy (500 eV, rastered area 400 × 400 μm^2). The sputter and analysis beams were turned on alternatively, giving in result a series of spectra acquired all along the depth of the sample.

XPS Analysis. Spectra were obtained using a VSW spectrometer equipped with a monochromatized X-ray source (Al Kα 1486.6 eV) in which the angle between the incident

https://doi.org/10.1021/acsomega.3c04266
ACS Omega 2023, 8, 28898−28909

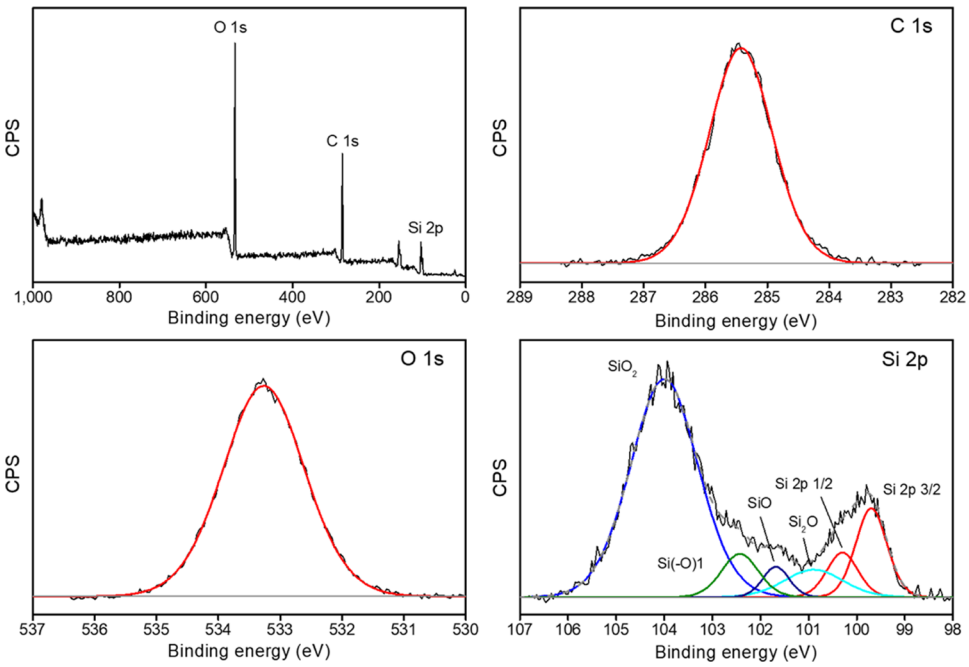

Figure 1. XPS spectra of the CH_3 long monolayer on porous silicon (survey spectra, C 1s, O 1s, and Si 2p core levels). XPS spectra of the other monolayers studied and of the bare porous silicon substrate are presented in the Supporting Information.

Table 3. XPS Atomic Percentages of C 1s, O 1s, Si 2p, and N 1s for porous SiO_2 Surface and for the Four Silane Monolayers on Porous Silicon

	C	O	N	Si	C/Si(−O)$_1$	Stoichiometric C/Si(−O)$_1$
SiO_2	1.6	50.7		47.7		
CH_3 short	14.6 ± 0.5	45.5 ± 1.0		39.9 ± 0.6	5.0	5
CH_3 long	41.6 ± 1.3	29.6 ± 0.1		28.8 ± 1.3	19.8	20
COO^-	28.9 ± 0.7	44.9 ± 0.5		26.2 ± 0.4	13.1	13
NH_3^+	16.6 ± 1.9	44.0 ±1.4	1.3 ± 1.0	38.1 ± 0.8	5.0	5

beam and the detector was the magic angle. The angular resolution was 3°. The take-off angle was 30° relative to the substrate surface. The energetic resolution was 0.2 eV. The data analysis was performed with CasaXPS software. Si(−O)$_4$ binding energy was set at 104 eV. A Shirley background was subtracted on Si 2p and O 1s spectra when coming from bulk elements while a linear background was subtracted on C 1s spectra as surface elements. Peaks were fitted by a Gauss−Lorentz curve.

SEM Imagery. SEM imaging of the matrix crystals was performed using a Mira 3 LMH (Tescan) with a Schottky tip and SE and BSE detectors. High vacuum mode was used for the images with an accelerating voltage of 2 kV. The spot size was around 8 nm with a current of 260 pA. On each surface, 1 μL of CHCA matrix at 10 mg/mL was deposited and let dry before SEM analysis. Four different droplets of the CHCA matrix were deposited on four different substrates (four replicates).

■ RESULTS AND DISCUSSION

Characterization of the Inter-Substrate Uniformity and Conformity of the Different Silane Monolayers. XPS spectra of the bare porous silicon surface and the four different monolayers are presented in Figures 1 and S1−S4. On the bare porous silicon surface, O 1s and Si 2p peaks are observed. On the high-resolution Si 2p spectra, the Si $2p_{1/2}$ and $2p_{3/2}$ contributions are associated to the bulk silicon, while the other contributions (SiO_2, Si_2O, and SiO) come from the oxidized layer at the silicon surface.[43] C 1s, O 1s, and Si 2p core levels are observed in the case of the four different silane monolayers, as well as the N 1s core level for the NH_3^+ monolayer. The Si(−O)$_1$ contribution observed on the Si 2p spectra is associated to the Si atom of the silane molecules. In the case of the NH_3^+ monolayer, a small contribution likely due to the C-N bond is observed on the C 1s spectra. The atomic percentages of each element are presented in Table 3. For each monolayer, the C 1s/Si(−O)$_1$ ratio is in accordance with the stoichiometric one.

An estimation of the surface coverage is obtained from the formula[44]

$$\Gamma_{\text{silanes}} = \frac{A_{\text{Si}(-\text{O})_1}}{A_{\text{Si}_{\text{silica}}}} n_{\text{SiO}_2} z \quad (1)$$

where z is the silica thickness (2 nm for native oxidation of the silicon surface), and n_{SiO_2} is the molecular concentration of silica (22 SiO_2 molecules/nm^3). $A_{\text{Si}(-\text{O})_1}$ and $A_{\text{Si}_{\text{silica}}}$ are the areas of the Si(−O)$_1$ peak and the total area of silica. The surface coverages obtained for each monolayer are presented in Table 4. This coverage is around four silane molecules/nm^2 except for the COO^- monolayer, for which the surface coverage is higher (5.4 molecules/nm^2). This could come from the longer silanisation process for this silane molecule compared with the other silane molecules (12 h for COO^- and 1 h for the other

https://doi.org/10.1021/acsomega.3c04266
ACS Omega 2023, 8, 28898−28909

Table 4. Surface Coverage Obtained by XPS for the Four Silane Monolayers on Porous Silicon[a]

	CH_3 short	CH_3 long	COO^-	NH_3^+
Surface coverage (silane/nm^2)	3.8 ± 0.4	4.1 ± 0.1	5.4 ± 0.1	4.4 ± 0.1

[a]Standard deviations are obtained from the measurement of three different samples.

silane molecules). The uniformity of the surface coverage was estimated by analyzing three different samples for each type of silane molecule. High uniformity was systematically obtained as figured out by the standard deviations indicated in Table 3.

Atomic percentages and surface coverage on plane silicon surfaces, functionalized with the four silane molecules studied, are similar to those obtained on porous silicon surfaces. These results have already been previously published by Lecot et al.[27]

ToF-SIMS depth profiling was used to characterize the conformity of the different silane monolayers on porous silicon surfaces. The depth profiles of the negative ions C^- (12.000 atomic mass unit [amu]) and $^{30}Si^-$ (29.9737 amu) are presented in Figure 2. While the intensity of $^{30}Si^-$ as a function of sputtering time is similar for the four surfaces (i.e., CH_3 short, CH_3 long, NH_3^+ silane monolayers, and bare porous silicon), the peak intensity of the C^- ion at 12 amu diverges depending on the surface. All along the depth profile and for all functionalized surfaces, its intensity was higher than on bare porous silicon suggesting the presence of the silane molecules inside the pores. Moreover, the NH^- ion profile confirms the presence of NH_3^+ silane molecules in the pore on the NH_3^+-functionalized surface (Figure S5). Finally, for all four silanes, the intensity of C^- ion remains steady until 4300 s of sputtering time, which suggests that the silane monolayers are evenly distributed inside the pores.

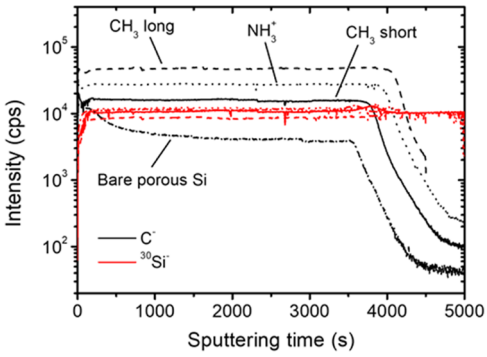

Figure 2. Depth profiling by ToF-SIMS of porous silicon functionalized by (solid) CH_3 short, (dash) CH_3 long, and (dot) NH_3^+ silane monolayers, and on (dash dot) bare porous silicon are presented. The intensities of the C^- ions (12 amu) and $^{30}Si^-$ (30 amu) ions as a function of sputtering are displayed in black and red, respectively. $^{30}Si^-$ ion in Si bulk (sputtering time greater than 4300 s) was used for normalization.

Detection of Sepsis Metabolites on Stainless-Steel Industrial Plates Using Different Organic Matrices. Classical stainless-steel MALDI target plates were used to select the matrix that allows the detection of the highest number of metabolites from the mixture solution containing 25 different metabolites. Six different matrices were studied: CHCA, DHB, 9AA, NEDC, THAP, and DAN. CHCA was shown to be the matrix that allows the simultaneous detection of the highest number of metabolites. Indeed, as shown in Figure 3, nine metabolites were detected at $[M + H]^+$. Consequently, the matrix CHCA was selected for the following analysis. Among these nine metabolites, LysoPC yields the highest S/N ratio at $[M + H]^+$ (S/N = 1304 at 524.4 m/z). Also, two of them (creatine and leucine) cannot be distinguished since they have the same mass and no fragments are detected. Moreover, several fragments of some metabolites, in particular of LysoPC, are detected, especially at 86.1 m/z ($(CH_3)N^+{-}CH{=}CH_2$), 104.1 m/z (choline), and 184.2 m/z (phosphocholine).[45] Nevertheless, in the following, only the peaks at $[M + H]^+$ for each metabolite are considered. It can be noticed that some metabolites, like LysoPC, are also well detected at $[M + H]^+$ using the DHB matrix. However, the S/N ratio of all of the metabolites detected using the CHCA matrix remains stable after a 1 h sample storage under vacuum, as well as after a 1 h sample storage in ambient conditions. On the contrary, the S/N ratio obtained using the DHB matrix decreases by more than 70% after 1 h storage.

The effects of the concentration of the CHCA matrix on the detection of LysoPC are presented in Figure 4. Five different concentrations were studied from 0 to 20 mg/mL. While no signal is obtained without the matrix, the $[M + H]^+$ peak intensity increases as the CHCA concentration increases up to 10 mg/mL. The same $[M + H]^+$ peak intensities are obtained at 10 and 20 mg/mL CHCA. So, in the following, a CHCA matrix at 10 mg/mL was used.

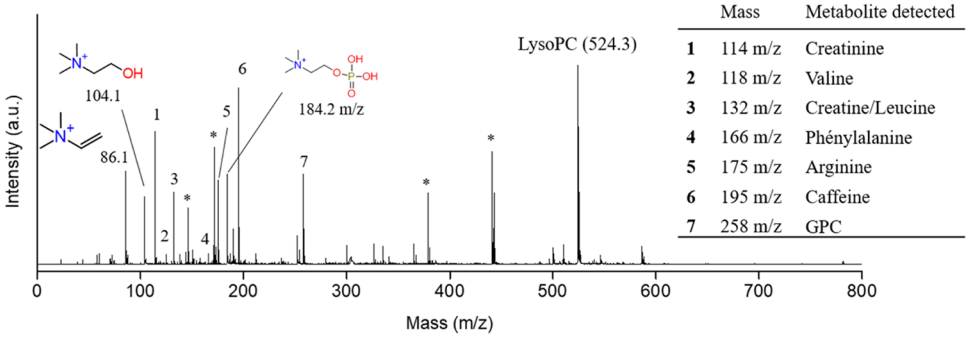

Figure 3. MALDI-ToF MS spectra of the mix of metabolites on a stainless-steel target plate with CHCA matrix. LysoPC is observed at 524.4 m/z ($[M + H]^+$) with fragments at 86.1 m/z, 104.1 m/z, and 184.2 m/z. The other metabolites detected are identified in the insert. Peaks were identified by comparison with the MALDI-ToF MS spectra of each metabolite alone in solution (results not shown). Matrix peaks are identified by a star.

https://doi.org/10.1021/acsomega.3c04266
ACS Omega 2023, 8, 28898−28909

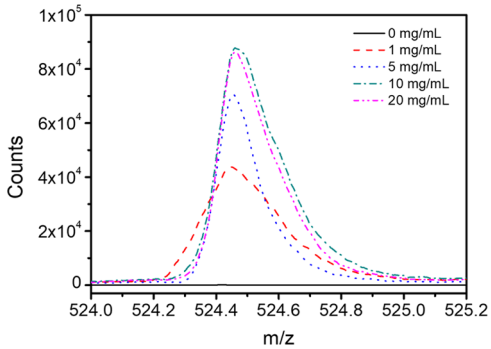

Figure 4. $[M + H]^+$ peak of LysoPC (524.4 m/z) for different concentrations of the CHCA matrix: 0 mg/mL (black solid), 1 mg/mL (red dash), 5 mg/mL (blue dot), 10 mg/mL (green dash dot), and 20 mg/mL (magenta dash dot).

Sepsis Metabolite Detection with and without Silane Monolayers on Plane and Porous Silicon Substrates. The effects of the different silane monolayers, on plane and porous silicon substrates, on the detection of sepsis metabolites, detected using the CHCA matrix, were investigated. Results were compared with the ones obtained with the bare plane and porous silicon surfaces and the ones obtained using the classical stainless-steel MALDI target plate. The corresponding mass spectra are presented in Figures 5 and 6. The $[M + H]^+$ peaks of the different metabolites are present on all of the surfaces studied with different intensities. To assess these differences, the S/N ratios, as well as the STD_{mean} and the intra-substrates uniformity obtained from the analysis of three different replicate samples, are determined for each surface (Table 5). The metabolites detected are presented in Table 5. Their octanol−water partition coefficient (log P) is in the range of −5.5−2.08 (for the most hydrophilic metabolite studied to the most hydrophobic one). Also, three of the detected metabolites have no global charge, while two of them have a high isoelectric point (10.77 and 8.99), and two of them have an isoelectric point of 6.4 and 6.33. Since creatine and leucine have the same mass and no fragments, they cannot be distinguished in the mass spectra. Also, these two molecules have very different isoelectric points and log P. Consequently, they are not considered in the following.

First, our results demonstrate that all of the metabolites detected on the stainless-steel target plate are also detected on the silanized and bare, plane and porous silicon substrates. In addition, two metabolites, glycine and alanine, not detected on the stainless-steel target plate can be detected by using silicon substrates. Indeed, alanine was detected on all silicon-based surfaces, while glycine was not detected on CH_3 short-modified porous silicon and bare plane silicon. Moreover, whatever the metabolite, except phenylalanine and valine, at least one of the silicon surfaces (plane or porous, bare or silanized) allows for improving the S/N value in comparison with the stainless-steel target plate. This first confirms that the choice of our silicon surfaces was appropriate. Second, these results demonstrate that there is no ideal silicon surface that proposes the best compromise for S/N, STD_{mean}, and intra-substrates uniformity for all of the metabolites. Depending on the chosen metabolite, planar or porous surfaces, as well as bare or silanized surfaces, are more suitable. Thus, the choice of a silicon surface allows to target the specificity to one of the metabolites. However, a mix of different silicon surfaces would be necessary to detect all of the metabolites for the

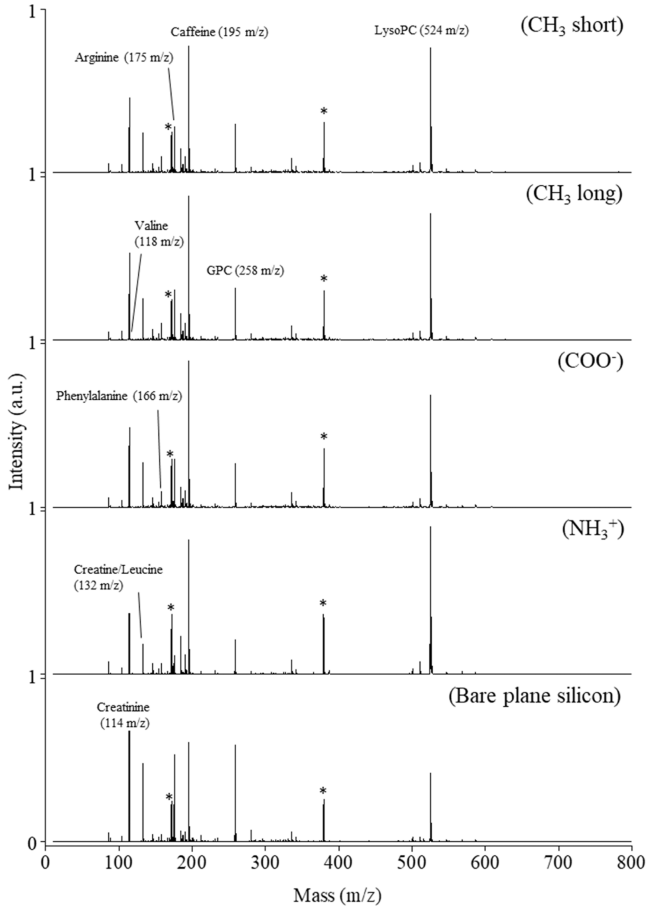

Figure 5. Mass spectra of the solution containing the mix of 25 metabolites, using CH_3 short, CH_3 long, COO^-, and NH_3^+ monolayers on plane silicon surfaces and using the bare plane silicon surface. Total ion count (TIC) normalization is used. Matrix peaks are identified by a star.

development of a sensing device. Nevertheless, it appears in Table 5 that substrates, planar or porous, functionalized with COO^- monolayers never present the best S/N ratio in comparison with the other silicon surfaces. Then, it appears that the COO^- monolayer is not an appropriate surface for the metabolites of our study, even if the uniformity and STD_{mean} values are often low and then induce a detection of the metabolites well controlled.

In detail, if we consider the STD_{mean}, results demonstrate that, when comparing the plane surfaces, out of the nine detected metabolites, NH_3^+-modified surfaces showed the worst STD_{mean} for seven metabolites (LysoPC, phenylalanine, valine, alanine, arginine, glycine, and GPC). Still, on plane substrates, bare silicon had the worst STD_{mean} for the remaining two metabolites (caffeine and creatinine). Using NH_3^+ porous silicon instead of NH_3^+ plane surfaces, the STD_{mean} was improved for all metabolites except for creatinine and valine.

To explain these results, the features of matrix crystallization on the different surfaces were studied by SEM. Figures S6−S14 present the SEM images of four replicates of the matrix droplets crystallized on each plane and porous substrate studied. Crystallization patterns on the plane substrates functionalized with the CH_3 short, CH_3 long, and COO^- monolayers and on the bare plane silicon surface were roughly similar from one replicate to another. However, matrix

https://doi.org/10.1021/acsomega.3c04266
ACS Omega 2023, 8, 28898−28909

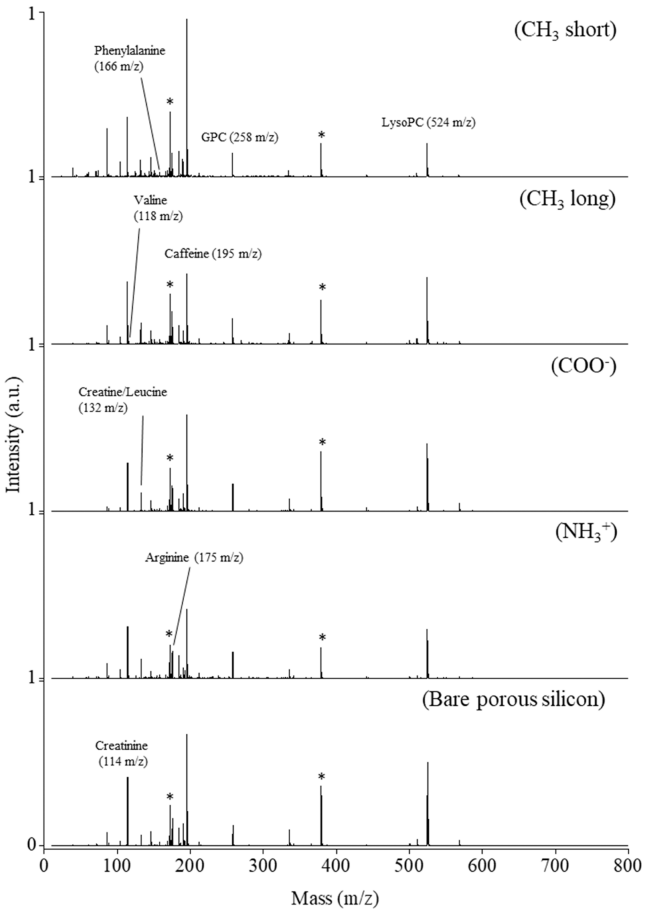

Figure 6. Mass spectra of the solution containing the mix of 25 metabolites, using CH_3 short, CH_3 long, COO^-, and NH_3^+ monolayers on porous silicon surfaces, and using the bare porous silicon surface. Total ion count (TIC) normalization is used. Matrix peaks are identified by a star.

crystallization features on the plane NH_3^+ monolayers varied. So matrix crystallization could explain the poor STD_{mean} of MALDI analysis in the case of the NH_3^+ monolayer on the plane silicon surface. Contrary to plane silicon surfaces, the shape of crystals on porous substrates appears to be similar whatever the type of silane monolayer, with the presence of dendrites. Also, the matrix crystallization features are similar on the four porous NH_3^+ monolayers studied. Consequently, matrix crystallization could explain the better STD_{mean} in MALDI analysis using the porous substrates functionalized with an NH_3^+ monolayer than the plane substrates.

In addition, CH_3 short monolayer on porous substrates in the case of creatinine and arginine leads to a worse STD_{mean} than the NH_3^+ monolayer on a plane silicon substrate, which is not correlated to the heterogeneity of matrix crystallization features. Thus, matrix crystallization features are not sufficient to systematically get a high STD_{mean} in MALDI analysis. Also, on porous substrates, the CH_3 short monolayer leads to better STD_{mean} and uniformity than the bare porous silicon substrate for LysoPC and phenylalanine, while the CH_3 long monolayer leads to better STD_{mean} and uniformity than the bare porous silicon substrate for valine, and the COO^- monolayer leads to better STD_{mean} than the bare porous silicon substrate for LysoPC, valine, alanine, and glycine. Thus, STD_{mean} and uniformity of analysis are likely due to a combination between the quality of matrix crystallization, the physicochemical properties of metabolites and surfaces, limitations in metabolite extraction from the pores because of mechanical constraints, and improvement in metabolite desorption due to the pores that could act as optimized laser energy receptacles.

If we consider the S/N ratio, the best ones are obtained on NH_3^+ monolayers and bare silicon for planar surfaces and on CH_3 short and long monolayers and bare silicon for porous silicon surfaces. If the bare silicon surface is a good candidate for the detection of many metabolites on planar and porous surfaces, it seems that the presence of pores modifies the detection ability of silanized surfaces. Indeed, the NH_3^+ monolayer is no more a good candidate on porous surfaces compared with planar surfaces. In fact, CH_3 short and long monolayers became more appropriate. It is such as the physicochemical properties of the surface are not the only determinant factors.

The most hydrophobic metabolites (LysoPC and caffeine) lead to higher S/N values by using the hydrophilic porous bare silicon substrate. These metabolites could be easily desorbed from hydrophilic surfaces and pores could act as optimized laser energy receptacles improving desorption. In the case of LysoPC, STD_{mean} and uniformity of the S/N values are demonstrated to be improved by using CH_3 short monolayers on porous and plane substrates.

Contrary to hydrophobic metabolites, the two most hydrophilic metabolites with the highest molecular masses (GPC and arginine) lead to higher S/N values using the bare plane silicon substrates than any other substrates. This result is in line with a previous study that has demonstrated that the MALDI-MS signal of hydrophilic analytes is higher on hydrophilic surfaces than on hydrophobic surfaces.[24,46] Also, hydrophilic pores could affect the extraction of hydrophilic metabolites, decreasing the S/N values in comparison with the plane silicon substrate.

In line with the results obtained for the most hydrophobic and hydrophilic metabolites, metabolites with intermediate log P (phenylalanine and creatinine) yield similar S/N values using plane and porous bare silicon substrates. In addition, STD_{mean} and uniformity of S/N values are improved by using a hydrophobic monolayer on the porous substrate (CH_3 short for phenylalanine) or on the plane substrate (CH_3 long for creatinine).

Finally, hydrophilic metabolites with the lowest molecular mass (glycine, alanine, and valine) lead to poor S/N values, on both plane and porous substrates, while improved STD_{mean} and uniformity are obtained by using the most hydrophobic plane substrates. Indeed, in the case of valine, the best uniformity and STD_{mean} are obtained on plane silicon substrates modified with CH_3 short monolayer (47 and 4, respectively). In the case of alanine, the best uniformity is obtained on the plane silicon substrates modified with CH_3 short and CH_3 long monolayers (47 in both cases), while the best STD_{mean} is obtained on the plane silicon substrates modified with CH_3 long monolayers (6). In the case of glycine, the CH_3 long-modified plane silicon surface is the best compromise to optimize both the STD_{mean} and the uniformity. Indeed, this substrate leads to the best STD_{mean} (10), even if an identical uniformity is obtained with the COO^--modified porous silicon substrate, and a uniformity of 73, very close to the best uniformity (72) obtained with the bare porous silicon substrate.

Beyond the effects of matrix crystallization and of the physicochemical properties of the substrates and metabolites, the effect of metabolite trapping inside the pores was

https://doi.org/10.1021/acsomega.3c04266
ACS Omega 2023, 8, 28898−28909

Table 5. S/N Ratio and Associated STD_{mean} (%) and Intra-Substrates Uniformity (%) for All of the Metabolites Simultaneously Detected on the Different Surfaces Studied, Using CHCA as a Matrix[a]

						Plane substrates					Porous substrates				
	m/z	Log P	IP	S/N stainless steel		CH_3 short	CH_3 long	COO^-	NH_3^+	Bare Si	CH_3 short	CH_3 long	COO^-	NH_3^+	Bare Si
LysoPC	524	2.1	NA	678	**S/N**	563	531	540	640	319	**536**	666	596	461	**806**
					uniformity	16	18	17	20	28	**15**	26	24	35	**17**
					STD_{mean}	4	7	3	20	15	**3**	5	9	17	**15**
Caffeine	195	-0.1	NA	521	**S/N**	562	563	570	618	506	632	430	379	370	**763**
					uniformity	25	27	24	32	30	23	33	46	41	**25**
					STD_{mean}	5	6	4	18	23	5	6	21	8	**4**
Phenylalanine	166	-1.2	6.33	34	**S/N**	12	11	10	14	14	**22**	16	8	20	13
					uniformity	29	28	27	38	34	**17**	23	33	35	24
					STD_{mean}	7	3	5	28	25	**1**	5	14	6	8
Creatinine	114	-1.4	8.99	566	**S/N**	885	**870**	830	753	924	756	588	632	513	**1027**
					uniformity	28	**29**	29	30	35	33	37	49	57	**28**
					STD_{mean}	7	**2**	1	10	13	22	6	21	12	**15**
Valine	118	-1.9	6.4	8	**S/N**	**7**	5	5	**8**	5	3	6	3	5	3
					uniformity	**47**	59	67	**71**	72	135	64	128	132	114
					STD_{mean}	**4**	6	11	**51**	23	34	17	12	67	40
Alanine	89	-2.8	6.1	ND	**S/N**	8	**7**	6	**10**	6	3	8	4	3	4
					uniformity	47	**47**	73	**75**	79	155	80	91	149	80
					STD_{mean}	11	**6**	13	**66**	31	45	15	8	13	20
Arginine	175	-3.1	10.77	256	**S/N**	299	270	235	228	**596**	280	228	163	171	395
					uniformity	28	36	30	32	**31**	35	36	43	40	23
					STD_{mean}	14	7	7	20	**1**	27	11	19	17	3
Glycine	75	-3.4	5.8	ND	**S/N**	4	**4**	3	**6**	ND	ND	5	4	3	3
					uniformity	77	**73**	116	**113**	ND	ND	75	80	188	72
					STD_{mean}	16	**10**	20	**89**	ND	ND	21	10	18	26
GPC	258	-5.5	NA	249	**S/N**	245	234	205	204	**426**	200	158	127	134	173
					uniformity	28	31	29	33	**30**	27	24	30	36	27
					STD_{mean}	8	4	8	17	**5**	16	6	13	4	11

[a] *m/z*, log *P*, and the isoelectric point (IP) are indicated for each metabolite. For a given metabolite, a substrate leading both to the highest S/N ratio and to the best compromise for STD_{mean} and uniformity is identified by red values. If such a substrate does not exist, the substrate leading to the highest S/N value is identified by bold black values and the substrate leading to the best compromise for STD_{mean} and uniformity is identified by green values. ND means not detected.

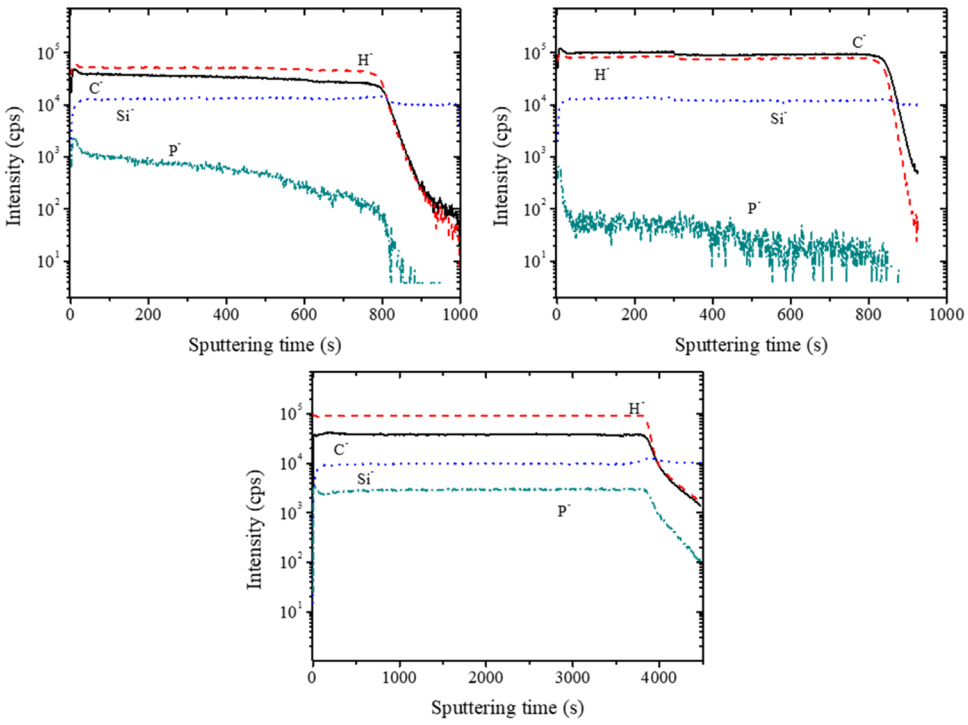

Figure 7. Depth profiling of C^-, H^-, Si^-, and P^- ions by ToF-SIMS on porous silicon functionalized by CH_3 short (left) and CH_3 long (right) silane monolayers, and on bare porous silicon (below). P^- ions are specific to the LysoPC molecule.

https://doi.org/10.1021/acsomega.3c04266
ACS Omega 2023, 8, 28898−28909

evaluated. LysoPC molecules were shown, by ToF-SIMS depth profiling analysis, to be trapped inside the pores of the CH_3 short substrate, and in the pores of the bare silicon substrate, while they stay at the surface of the CH_3 long substrate (Figure 7). However, LysoPC trapping inside the pores seems to have only a little impact on the STD_{mean} and intra-substrates uniformity, which is slightly better for CH_3 short (LysoPC inside the pores) than for CH_3 long monolayers (LysoPC outside the pores), despite a lower S/N ratio in the case of CH_3 short monolayers. In addition, our results suggest that hydrophobic pores may act as optimized energy receptacles improving the S/N values for LysoPC molecules when localize on the surface outside the pores, while this effect is counterbalanced by mechanical constraints impeding LysoPC molecules when the molecules are trapped inside the pores. Indeed, the S/N value for LysoPC is higher on the CH_3 long-modified porous substrates than on the CH_3 long-modified plane substrates (666 and 531, respectively). Also, the S/N value for LysoPC is lower on the CH_3 short-modified porous substrate than on the CH_3 long-modified porous substrates (536 and 666, respectively). Finally, the difference between the S/N values for LysoPC on the CH_3 short-modified plane and porous substrates (563 and 536, respectively) is lower than the difference between the S/N values for LysoPC on the CH_3 long-modified plane and porous substrates (531 and 666, respectively).

CONCLUSIONS

The CHCA matrix was shown to allow the simultaneous detection, on the classical stainless-steel MALDI target plate, of 9 metabolites among the 25 metabolites studied, while 2 more metabolites are detected on the silanized and bare silicon substrates. LysoPC is the metabolite that leads to the highest signal intensity. The features of the CHCA matrix crystals were demonstrated to vary further on plane substrates than on porous substrates, especially on plane NH_3^+ substrates. Nevertheless, in the case of porous substrates, the presence and the type of silane monolayers do not impact the matrix crystallization. The quality of matrix crystals is demonstrated to be in line with the poor STD_{mean} of MALDI analysis obtained with the NH_3^+ monolayer on plane silicon substrates and also with the better STD_{mean} obtained on the NH_3^+ monolayer on porous substrates than on plane substrates. Nevertheless, in the case of the other monolayers, no correlation was found between the STD_{mean} of the S/N values and matrix crystal features. Thus, results suggest that MALDI analysis depends on a complex combination of several factors such as the quality of matrix crystallization, the physicochemical properties of metabolites and surfaces, and the presence of pores. Moreover, our results demonstrate that porous silicon may have two opposite effects on the MALDI signal. On the one hand, it serves as an energy receptacle of the incident light which favors the desorption/ionization of the molecules. On the other hand, it physically traps the molecules preventing them from escaping from the surface if these molecules are localized deep inside the pores. In the case of the most hydrophobic metabolites studied, LysoPC and caffeine, the highest S/N ratio was obtained using the bare (hydrophilic) porous silicon substrates. However, CH_3 short monolayer on porous substrates could be a good trade-off to optimize both the S/N ratio of LysoPC and the associated intra-substrate uniformity and STD_{mean}. In the case of the most hydrophilic metabolites with the highest molecular masses (GPC and arginine), the highest S/N ratio was observed on bare plane silicon. For the lowest molecular weight (valine, alanine, and glycine), the S/N ratio was lower than 11 on all surfaces, but the STD_{mean} or the uniformity was improved on CH_3 long or CH_3 short silane-modified plane substrates. Finally, metabolites with intermediate log P (phenylalanine and creatinine) yield the best MALDI analysis by a using hydrophobic monolayer on the porous substrate (CH_3 short for phenylalanine) or on the plane substrate (CH_3 long for creatinine).

These results would need to be extended in plasma samples, where the abundant large molecules will be sterically excluded from the pores and removed from the surface by water washing. Then, a reduced number of substrates could be selected to improve the MALDI-ToF MS detection of the panel of sepsis metabolites. In addition, to further increase the number of metabolites detected among the 25 metabolites studied, and also to further improve the limit of detection, DIOS-MS strategy, based on silanized porous silicon substrates, could be investigated.[47] Indeed, for instance, a slight CHCA matrix peak interferes with the $[M + H]^+$ peak of LysoPC, limiting its detection to around 0.5 ng/mL in the mix of metabolites studied. However, the physiological concentration of LysoPC is far above this detection limit, around 40 ng/mL, and decreases in the case of sepsis. So, the substrates studied, easily marketable at low cost and high throughput, could be promising to develop a strategy for sepsis diagnosis in a few minutes, without any pretreatment protocols of the samples, based on sepsis metabolites MALDI-ToF MS analysis.

ASSOCIATED CONTENT

Supporting Information

The Supporting Information is available free of charge at https://pubs.acs.org/doi/10.1021/acsomega.3c04266.

XPS spectra of the porous SiO_2 surface, CH_3 short monolayer, COO^- monolayer, and NH_3^+ monolayer on porous silicon. Depth profiling of silicon and NH ions by ToF-SIMS on porous silicon functionalized by NH_3^+ silane monolayer and on bare porous silicon. SEM image of CHCA matrix deposition on plane silicon with CH_3 short silane monolayer, CH_3 long silane monolayer, COO^- silane monolayer, and NH_3^+ silane monolayer. SEM image of CHCA matrix deposition on porous silicon with CH_3 short silane monolayer, CH_3 long silane monolayer, COO^- silane monolayer, and NH_3^+ silane monolayer. SEM image of CHCA matrix deposition on bare porous silicon (PDF)

AUTHOR INFORMATION

Corresponding Author

Christelle Yeromonahos − *Univ Lyon, Ecole Centrale de Lyon, CNRS, INSA Lyon, Université Claude Bernard Lyon 1, CPE Lyon, INL, UMR5270, 69134 Ecully Cedex, France;* orcid.org/0000-0002-1326-3091; Phone: + 33 4 72 18 62 35; Email: christelle.yeromonahos@ec-lyon.fr

Authors

Antonin Lavigne − *Univ Lyon, Ecole Centrale de Lyon, CNRS, INSA Lyon, Université Claude Bernard Lyon 1, CPE Lyon, INL, UMR5270, 69134 Ecully Cedex, France*

Thomas Géhin − *Univ Lyon, CNRS, Ecole Centrale de Lyon, INSA Lyon, Université Claude Bernard Lyon 1, CPE Lyon, INL, UMR5270, 69134 Ecully Cedex, France*

https://doi.org/10.1021/acsomega.3c04266
ACS Omega 2023, 8, 28898−28909

Benoît Gilquin − *Univ Grenoble Alpes, CEA, LETI, F-38000 Grenoble, France*
Vincent Jousseaume − *Univ Grenoble Alpes, CEA, LETI, F-38000 Grenoble, France*
Marc Veillerot − *Univ Grenoble Alpes, CEA, LETI, F-38000 Grenoble, France*
Claude Botella − *Univ Lyon, CNRS, Ecole Centrale de Lyon, INSA Lyon, Université Claude Bernard Lyon 1, CPE Lyon, INL, UMR5270, 69134 Ecully Cedex, France*
Céline Chevalier − *Univ Lyon, INSA Lyon, CNRS, Ecole Centrale de Lyon, Université Claude Bernard Lyon 1, CPE Lyon, INL, UMR5270, 69621 Villeurbanne Cedex, France*
Cécile Jamois − *Univ Lyon, INSA Lyon, CNRS, Ecole Centrale de Lyon, Université Claude Bernard Lyon 1, CPE Lyon, INL, UMR5270, 69621 Villeurbanne Cedex, France*
Yann Chevolot − *Univ Lyon, CNRS, Ecole Centrale de Lyon, INSA Lyon, Université Claude Bernard Lyon 1, CPE Lyon, INL, UMR5270, 69134 Ecully Cedex, France;* orcid.org/0000-0003-3479-3371
Magali Phaner-Goutorbe − *Univ Lyon, Ecole Centrale de Lyon, CNRS, INSA Lyon, Université Claude Bernard Lyon 1, CPE Lyon, INL, UMR5270, 69134 Ecully Cedex, France*

Complete contact information is available at:
https://pubs.acs.org/10.1021/acsomega.3c04266

Author Contributions

The manuscript was written through the contributions of all authors. All authors have given approval to the final version of the manuscript.

Funding

This work was supported by the Young Researcher ANR PORIDG Project, Grant ANR-18-CE09-0006 of the French Agence Nationale de la Recherche.

Notes

The authors declare no competing financial interest.

■ ACKNOWLEDGMENTS

A.L. is grateful to the ANR PORIDG, of the French Agence Nationale de la Recherche, for funding his Ph.D. fellowship.

■ REFERENCES

(1) Huang, Y.; Du, S.; Liu, J.; Huang, W.; Liu, W.; Zhang, M.; Li, N.; Wang, R.; Wu, J.; Chen, W.; et al. Diagnosis and Prognosis of Breast Cancer by High-Performance Serum Metabolic Fingerprints. *Proc. Natl. Acad. Sci. U.S.A.* **2022**, *119*, No. e2122245119.
(2) Kulkarni, A. S.; Huang, L.; Qian, K. Material-Assisted Mass Spectrometric Analysis of Low Molecular Weight Compounds for Biomedical Applications. *J. Mater. Chem. B* **2021**, *9*, 3622−3639.
(3) Li, D.; Yi, J.; Han, G.; Qiao, L. MALDI-TOF Mass Spectrometry in Clinical Analysis and Research. *ACS Meas. Sci. Au* **2022**, *2*, 385−404.
(4) Iakab, S. A.; Rafols, P.; García-Altares, M.; Yanes, O.; Correig, X. Silicon-Based Laser Desorption Ionization Mass Spectrometry for the Analysis of Biomolecules: A Progress Report. *Adv. Funct. Mater.* **2019**, *29*, No. 1903609.
(5) Müller, W. H.; De Pauw, E.; Far, J.; Malherbe, C.; Eppe, G. Imaging Lipids in Biological Samples with Surface-Assisted Laser Desorption/Ionization Mass Spectrometry: A Concise Review of the Last Decade. *Prog. Lipid Res.* **2021**, *83*, No. 101114.
(6) Fincher, J. A.; Korte, A. R.; Yadavilli, S.; Morris, N. J.; Vertes, A. Multimodal Imaging of Biological Tissues Using Combined MALDI and NAPA-LDI Mass Spectrometry for Enhanced Molecular Coverage. *Analyst* **2020**, *145*, 6910−6918.
(7) Northen, T. R.; Yanes, O.; Northen, M. T.; Marrinucci, D.; Uritboonthai, W.; Apon, J.; Golledge, S. L.; Nordström, A.; Siuzdak, G. Clathrate Nanostructures for Mass Spectrometry. *Nature* **2007**, *449*, 1033−1036.
(8) Greving, M. P.; Patti, G. J.; Siuzdak, G. Nanostructure-Initiator Mass Spectrometry Metabolite Analysis and Imaging. *Anal. Chem.* **2011**, *83*, 2−7.
(9) Qiao, Z.; Lissel, F. MALDI Matrices for the Analysis of Low Molecular Weight Compounds: Rational Design, Challenges and Perspectives. *Chem. − Asian J.* **2021**, *16*, 868−878.
(10) Moening, T. N.; Brown, V. L.; He, L. Matrix-Enhanced Nanostructure Initiator Mass Spectrometry (ME-NIMS) for Small Molecule Detection and Imaging. *Anal. Methods* **2016**, *8*, 8234−8240.
(11) Jousseaume, V.; El Sabahy, J.; Yeromonahos, C.; Castellan, G.; Bouamrani, A.; Ricoul, F. SiOCH Thin Films Deposited by Chemical Vapor Deposition: From Low-κ to Chemical and Biochemical Sensors. *Microelectron. Eng.* **2017**, *167*, 69−79.
(12) Mombrun, A.; Bouamrani, M.-A.; Boyer, E.; Yeromonahos, C. Device for In Vivo Sampling of Biological Species. WIPO Patent WO2015166019A1, 2015.
(13) Kaderbay, A.; Berger, F.; Bouamrani, A.; Bidart, M.; Petre, G.; Baguant, A.; Giraud, L.; Schmerber, S. Perilymph Metabolomic and Proteomic MALDI-ToF Profiling with Porous Silicon Chips: A Proof-of-Concept Study. *Hear. Res.* **2022**, *417*, No. 108457.
(14) Bouamrani, A.; Hu, Y.; Tasciotti, E.; Li, L.; Chiappini, C.; Liu, X.; Ferrari, M. Mesoporous Silica Chips for Selective Enrichment and Stabilization of Low Molecular Weight Proteome. *Proteomics* **2010**, *10*, 496−505.
(15) Wang, X.; Teng, F.; Wang, Y.; Lu, N. Rapid Liquid-Phase Microextraction of Analytes from Complex Samples on Superwetting Porous Silicon for Onsite SALDI-MS Analysis. *Talanta* **2019**, *198*, 63−70.
(16) Ma, C.; Xie, L.; Wang, X.; Liang, K.; Kong, B. Interfacial Assembly of Functional Mesoporous Nanomatrices for Laser Desorption/Ionization Mass Spectrometry. *Nano Today* **2022**, *42*, No. 101365.
(17) Ma, S.; Zhang, L.; Wang, S.; Zhang, H.; You, X.; Ou, J.; Ye, M.; Wei, Y. Preparation of Epoxy-Functionalized Hierarchically Porous Hybrid Monoliths via Free Radical Polymerization and Application in HILIC Enrichment of Glycopeptides. *Anal. Chim. Acta* **2019**, *1058*, 97−106.
(18) Tian, Y.; Tang, R.; Liu, L.; Yu, Y.; Ma, S.; Gong, B.; Ou, J. Glutathione-Modified Ordered Mesoporous Silicas for Enrichment of N-Linked Glycopeptides by Hydrophilic Interaction Chromatography. *Talanta* **2020**, *217*, No. 121082.
(19) Sun, J.; Yu, G.; Yang, Y.; Qiao, L.; Xu, B.; Ding, C.; Liu, Y.; Yu, S. Evaluation of Prostate Cancer Based on MALDI-TOF MS Fingerprinting of Nanoparticle-Treated Serum Proteins/Peptides. *Talanta* **2020**, *220*, No. 121331.
(20) Li, N.; Dou, S.; Feng, L.; Zhu, Q.; Lu, N. Eliminating Sweet Spot in MALDI-MS with Hydrophobic Ordered Structure as Target for Quantifying Biomolecules. *Talanta* **2020**, *218*, No. 121172.
(21) Dou, S.; Li, N.; Wang, X.; Zhu, Q.; Wang, Z.; Lu, N. Self-Assembly of Super-Hydrophobic PMMA Microspheres on Silicon Wafer as MALDI-MS Chip for Rapid Quantification of Peptides. *Sens. Actuators, B* **2020**, *306*, No. 127573.
(22) Zhou, H.; Xu, S.; Ye, M.; Feng, S.; Pan, C.; Jiang, X.; Li, X.; Han, G.; Fu, Y.; Zou, H. Zirconium Phosphonate-Modified Porous Silicon for Highly Specific Capture of Phosphopeptides and MALDI-TOF MS Analysis. *J. Proteome Res.* **2006**, *5*, 2431−2437.
(23) Xu, Y.; Wu, Z.; Zhang, L.; Lu, H.; Yang, P.; Webley, P. A.; Zhao, D. Highly Specific Enrichment of Glycopeptides Using Boronic Acid-Functionalized Mesoporous Silica. *Anal. Chem.* **2009**, *81*, 503−508.
(24) Hsieh, S.; Ku, H.-Y.; Ke, Y.-T.; Wu, H.-F. Self-Assembled-Monolayer-Modified Silicon Substrate to Enhance the Sensitivity of Peptide Detection for AP-MALDI Mass Spectrometry. *J. Mass Spectrom.* **2007**, *42*, 1628−1636.

(25) Lecot, S.; Chevolot, Y.; Phaner-Goutorbe, M.; Yeromonahos, C. Impact of Silane Monolayers on the Adsorption of Streptavidin on Silica and Its Subsequent Interactions with Biotin: Molecular Dynamics and Steered Molecular Dynamics Simulations. *J. Phys. Chem. B* **2020**, *124*, 6786−6796.
(26) Lecot, S.; Chevolot, Y.; Phaner-Goutorbe, M.; Yeromonahos, C. Curious Binding Energy Increase between the Receptor-Binding Domain of the SARS-CoV-2 Spike Protein and Angiotensin-Converting Enzyme 2 Adsorbed on a Silane Monolayer from Molecular Dynamics Simulations. *J. Phys. Chem. B* **2021**, *125*, 11078−11090.
(27) Lecot, S.; Lavigne, A.; Yang, Z.; Géhin, T.; Botella, C.; Jousseaume, V.; Chevolot, Y.; Phaner-Goutorbe, M.; Yeromonahos, C. Arrangement of Monofunctional Silane Molecules on Silica Surfaces: Influence of Alkyl Chain Length, Head-Group Charge, and Surface Coverage, from Molecular Dynamics Simulations, X-Ray Photoelectron Spectroscopy, and Fourier Transform Infrared Spectroscopy. *J. Phys. Chem. C* **2020**, *124*, 20125−20134.
(28) Lecot, S.; Lavigne, A.; Yang, Z.; Chevolot, Y.; Phaner-Goutorbe, M.; Yeromonahos, C. Effects of the Chemical and Structural Properties of Silane Monolayers on the Organization of Water Molecules and Ions at Interfaces, from Molecular Dynamics Simulations. *Langmuir* **2021**, *37*, 5563−5572.
(29) Wang, J.; Sun, Y.; Teng, S.; Li, K. Prediction of Sepsis Mortality Using Metabolite Biomarkers in the Blood: A Meta-Analysis of Death-Related Pathways and Prospective Validation. *BMC Med.* **2020**, *18*, 83.
(30) Neugebauer, S.; Giamarellos-Bourboulis, E. J.; Pelekanou, A.; Marioli, A.; Baziaka, F.; Tsangaris, I.; Bauer, M.; Kiehntopf, M. Metabolite Profiles in Sepsis: Developing Prognostic Tools Based on the Type of Infection. *Crit. Care Med.* **2016**, *44*, 1649−1662.
(31) Park, J.-M.; Noh, J.-Y.; Kim, M.-J.; Yun, T. G.; Lee, S.-G.; Chung, K. S.; Lee, E. H.; Shin, M. H.; Ku, N. S.; Yoon, S.; et al. MALDI-TOF Mass Spectrometry Based on Parylene-Matrix Chip for the Analysis of Lysophosphatidylcholine in Sepsis Patient Sera. *Anal. Chem.* **2019**, *91*, 14719−14727.
(32) Lee, E. H.; Shin, M. H.; Park, J.-M.; Lee, S.-G.; Ku, N. S.; Kim, Y. S.; Park, M. S.; Pyun, J.-C.; Chung, K. S. Diagnosis and Mortality Prediction of Sepsis via Lysophosphatidylcholine 16:0 Measured by MALDI-TOF MS. *Sci. Rep.* **2020**, *10*, No. 13833.
(33) Drobnik, W.; Liebisch, G.; Audebert, F.-X.; Fröhlich, D.; Glück, T.; Vogel, P.; Rothe, G.; Schmitz, G. Plasma Ceramide and Lysophosphatidylcholine Inversely Correlate with Mortality in Sepsis Patients. *J. Lipid Res.* **2003**, *44*, 754−761.
(34) Kauppi, A. M.; Edin, A.; Ziegler, I.; Mölling, P.; Sjöstedt, A.; Gylfe, Å.; Strålin, K.; Johansson, A. Metabolites in Blood for Prediction of Bacteremic Sepsis in the Emergency Room. *PLoS One* **2016**, *11*, No. e0147670.
(35) Su, L.; Li, H.; Xie, A.; Liu, D.; Rao, W.; Lan, L.; Li, X.; Li, F.; Xiao, K.; Wang, H.; et al. Dynamic Changes in Amino Acid Concentration Profiles in Patients with Sepsis. *PLoS One* **2015**, *10*, No. e0121933.
(36) Wexler, O.; Gough, M. S.; Morgan, M. A. M.; Mack, C. M.; Apostolakos, M. J.; Doolin, K. P.; Mooney, R. A.; Arning, E.; Bottiglieri, T.; Pietropaoli, A. P. Methionine Metabolites in Patients With Sepsis. *J. Intensive Care Med.* **2018**, *33*, 37−47.
(37) Zhou, Y.; Dong, H.; Zhong, Y.; Huang, J.; Lv, J.; Li, J. The Cold-Inducible RNA-Binding Protein (CIRP) Level in Peripheral Blood Predicts Sepsis Outcome. *PLoS One* **2015**, *10*, No. e0137721.
(38) Asaduzzaman, M.; Ahmed, M. N. U.; Rahman, A. F.; Reza, S. T.; Afifa, M.; Ahmed, B. W.; Asaduzzaman, M. Role of Glucose Variability in the Diagnosis of Septic Patients. *Bangladesh Crit. Care J.* **2022**, *10*, 10−14.
(39) Marshall, J. C. Biomarkers of Sepsis. *Curr. Infect. Dis. Rep.* **2006**, *8*, 351−357.
(40) Dugas, V.; Depret, G.; Chevalier, Y.; Nesme, X.; Souteyrand, É. Immobilization of Single-Stranded DNA Fragments to Solid Surfaces and Their Repeatable Specific Hybridization: Covalent Binding or Adsorption? *Sens. Actuators, B* **2004**, *101*, 112−121.
(41) Phaner-Goutorbe, M.; Dugas, V.; Chevolot, Y.; Souteyrand, E. Silanization of Silica and Glass Slides for DNA Microarrays by Impregnation and Gas Phase Protocols: A Comparative Study. *Mater. Sci. Eng. C* **2011**, *31*, 384−390.
(42) Cerruti, C. D.; Benabdellah, F.; Laprévote, O.; Touboul, D.; Brunelle, A. MALDI Imaging and Structural Analysis of Rat Brain Lipid Negative Ions with 9-Aminoacridine Matrix. *Anal. Chem.* **2012**, *84*, 2164−2171.
(43) Ghita, R.; Logofatu, C.; Negrila, C.-C.; Ungureanu, F.; Cotirlan, C.; Manea, A.-S.; Lazarescu, M.-F.; Ghic, C. Study of SiO_2/Si Interface by Surface Techniques. In *Crystalline Silicon − Properties and Uses*; Basu, S., Ed.; InTech: Rijeka, 2011; pp 23−42.
(44) Shircliff, R. A.; Martin, I. T.; Pankow, J. W.; Fennell, J.; Stradins, P.; Ghirardi, M. L.; Cowley, S. W.; Branz, H. M. High-Resolution X-Ray Photoelectron Spectroscopy of Mixed Silane Monolayers for DNA Attachment. *ACS Appl. Mater. Interfaces* **2011**, *3*, 3285−3292.
(45) Chughtai, K.; Jiang, L.; Greenwood, T. R.; Glunde, K.; Heeren, R. M. A. Mass Spectrometry Images Acylcarnitines, Phosphatidylcholines, and Sphingomyelin in MDA-MB-231 Breast Tumor Models. *J. Lipid Res.* **2013**, *54*, 333−344.
(46) Trauger, S. A.; Go, E. P.; Shen, Z.; Apon, J. V.; Compton, B. J.; Bouvier, E. S. P.; Finn, M. G.; Siuzdak, G. High Sensitivity and Analyte Capture with Desorption/Ionization Mass Spectrometry on Silylated Porous Silicon. *Anal. Chem.* **2004**, *76*, 4484−4489.
(47) Lavigne, A.; Gilquin, B.; Géhin, T.; Jousseaume, V.; Veillerot, M.; Chevolot, Y.; Phaner-Goutorbe, M.; Yeromonahos, C. Effects of Silane Monolayers on Lysophosphatidylcholine (LysoPC) Detection by Desorption Ionization on Silicon Mass Spectrometry (DIOS-MS) in Solution and Plasma. *ACS Appl. Mater. Interfaces* **2023**, *15*, 18685−18693.

https://doi.org/10.1021/acsomega.3c04266
ACS Omega 2023, 8, 28898−28909